ISSN 1674-1056
http://cpb.iphy.ac.cn
http://iopscience.iop.org/cpb
中国物理 B
Chinese Physics
中国物理
Chinese Physics B

Electron transport properties of TiO_2 shell on Al_2O_3 core in dye-sensitized solar cells

Dongmei Xie(解东梅), Xiaowen Tang(唐小文), Yuan Lin(林原), Pin Ma(马品), Xiaowen Zhou(周晓文)
Citation: Chin. Phys. B . 2018, 27(1): 017804. **doi:** 10.1088/1674-1056/27/1/017804

Journal homepage: http://cpb.iphy.ac.cn; http://iopscience.iop.org/cpb

What follows is a list of articles you may be interested in

Electron transport properties of TiO_2 shell on Al_2O_3 core in dye-sensitized solar cells

Dongmei Xie(解东梅), Xiaowen Tang(唐小文), Yuan Lin(林原), Pin Ma(马品), Xiaowen Zhou(周晓文)
Chin. Phys. B . 2018, 27(1): 017803. **doi:** 10.1088/1674-1056/27/1/017803

First-principles hybrid functional study of the electronic structure and charge carrier mobility in perovskite $CH_3NH_3SnI_3$

Li-Juan Wu(伍丽娟), Yu-Qing Zhao(赵宇清), Chang-Wen Chen(陈畅文), Ling-Zhi Wang(王琳芝), Biao Liu(刘标), Meng-Qiu Cai(蔡孟秋)
Chin. Phys. B . 2016, 25(10): 107202. **doi:** 10.1088/1674-1056/25/10/107202

Effect of CuPc and MoO_3 co-evaporated layer on the conductivity of organic light emitting diodes

He Ze-Shang, Yu Hao-Miao, Peng Huan, Hou Xiao-Yuan
Chin. Phys. B . 2015, 24(9): 097201. **doi:** 10.1088/1674-1056/24/9/097201

Raman scattering in In/InO_x core–shell structured nanoparticles

Wang Meng, Tian Ye, Zhang Jian-Ming, Guo Chuan-Fei, Zhang Xin-Zheng, Liu Qian
Chin. Phys. B . 2014, 23(8): 087803. **doi:** 10.1088/1674-1056/23/8/087803

Electric field-induced hole injection-enhanced photoluminescence in a N,N'-bis(3-methylphenyl)-N,N'-bis(phenyl)-benzidine-based emitter

Xu-Xie Hui-Na, Li Wen-Bin, Peng Huan, He Yun, Yu Hao-Miao, Hou Xiao-Yuan
Chin. Phys. B . 2014, 23(4): 047202. **doi:** 10.1088/1674-1056/23/4/047202

SPECIAL TOPIC — New generation solar cells

Electron transport properties of TiO_2 shell on Al_2O_3 core in dye-sensitized solar cells*

Dongmei Xie(解东梅)[1,2,#], Xiaowen Tang(唐小文)[1,2,#], Yuan Lin(林原)[1,2,†], Pin Ma(马品)[1,2], and Xiaowen Zhou(周晓文)[1,2]

[1] *Beijing National laboratory for Molecular Sciences, Key Laboratory of Photochemistry, CAS Research/Education Center for Excellence in Molecular Sciences, Institute of Chemistry, Chinese Academy of Sciences, Beijing* 100190, *China*
[2] *University of Chinese Academy of Sciences, Beijing* 100049, *China*

(Received 30 September 2017; revised manuscript received 13 November 2017; published online 22 December 2017)

The performance of dye-sensitized solar cells (DSSCs) is strongly affected by the properties of semiconductor nanoparticles. In this work, we used TiO_2 particles prepared by $TiCl_4$ hydrolysis n times on Al_2O_3 films (A/T(n)), and investigated morphology, photoelectric, and electron transport properties of A/T(n). The TiO_2 shell was composed of 10–20 nm nanoparticles and the number of nanoparticles increased with increasing $TiCl_4$ treatment times. The highest photoelectric conversion efficiency of 3.23% was obtained as A/T(4). IMPS results indicated that electron transport rate was high enough to conduct current, and was not the dominating effect to limit the J_{sc}. J_{sc} was mainly determined by dye loading on TiO_2 and the interconnection of TiO_2. These may provide a new strategy for preparing semiconductor working electrodes for DSSC.

Keywords: dye-sensitized solar cell, electron transportation, core–shell structure, intensity-modulated photocurrent spectroscopy

PACS: 78.55.Mb, 72.20.Jv, 84.60.Jt, 88.40.H– **DOI:** 10.1088/1674-1056/27/1/017804

1. Introduction

In the past 20 years, dye-sensitized solar cells (DSSCs) were intensively investigated by researchers and industries owing to their low cost, easy fabrication and high photoelectric conversion efficiency (PCE).[1–5]

DSSC consists of a wide-bandgap nanocrystal semiconductor anode, an electrolyte and a counter electrode.[6,7] In order to realize a high PCE, wide-bandgap semiconductors must satisfy the following requirements: (i) bandgap is larger than 3.2 eV to reduce the adsorption of visible light;[8] (ii) conduction band edge needs to align with the lowest unoccupied molecular orbital (LUMO) of the dye; (iii) carrier has the fast transport rate; (iv) the rate of recombination between electron in semiconductor and electrolyte is slow. Up to now, few materials can satisfy both requirements (iii) and (iv). TiO_2 has a slow electron recombination rate and a slow electron transport rate. On the contrary, ZnO[9–14] and SnO_2[15–19] have fast electron transport rates and a fast electron recombination rate. Among all the semiconductors, DSSCs with TiO_2 as anode have the highest PCE, larger than those with of ZnO and SnO_2. However, the electron transport rate in TiO_2 is lower than that of ZnO and SnO_2. In order to increase PCE of DSSCs, much research has been carried out on the understanding which makes the electron transport rate slow and how to improve the electron transport rate of TiO_2.

The transient current and intensity-modulated photocurrent spectroscopy (IMPS) are used to investigate electron transport properties in semiconductor nanocrystalline film. It is found that the electron transport rate is 1–3 orders of magnitude slower than that of bulk materials and proportional to the square root of electron density. Most popular trap–detrap models can explain these results. Electrons are trapped by defect states during the transport, and the trapped electrons need to be excited by heat to detrap to the conduction band to transport again. With the increase in electron density, the occupation of trapped states is increased, which makes rate of electron trap slower and detrap faster, and consequently the transport rate is increased. Moreover, the disordered distribution of nanoparticles increases the transport path length, then decreases the transport rate.

The core–shell structure is one of the possible methods to enhance electron transport rate. ZnO or SnO_2 nanoparticles covered by TiO_2 may combine the advantages of the high electron transport rate of the core and the low electron recombination rate of the shell. However, the result of the core–shell structure is not as good as we expected. This is because the energy level of the shell does not match with the core and the poor electronic contact between the core and shell, or the re-

*Project supported by the National Materials Genome Project of China (Grant No. 2016YFB0700600) and the National Natural Science Foundation of China (Grant No. 51673204).

#These authors contributed equally to this work.

†Corresponding author. E-mail: linyuan@iccas.ac.cn

© 2018 Chinese Physical Society and IOP Publishing Ltd

combination between core and electrolyte is not fully inhibited by the shell owing to poor morphology.

In this paper, we designed and fabricated the photoanode of DSSCs, which centered on an Al_2O_3 core surrounded by a TiO_2 shell (A/T(n)). We used this core–shell structure as a model to investigate the effect of electron transport rate on photoelectric properties of cells. J_{sc} and PCE peaked at A/T(4), with values of 7.79 mA·cm^{-2} and 3.32% respectively. This study provides a method to study the mechanism of electron transport in nanocrystalline porous film.

2. Experimental section

2.1. Preparation of TiO_2 compact layer

Isopropyl titanium (0.455 mL) was added to n-propanol (20 mL) to form a TiO_2 paste under stirring for 12 h at room temperature. The TiO_2 compact layer was prepared on the FTO plate using spin-coating technique, and then was heated at 450 °C for 30 min.

2.2. Preparation of A/T(n) photoanode

Al_2O_3 (0.4 g), triton-100 (0.2 g), acetic acid (0.4 ml), and deionized water (2 ml) were first mixed to form the Al_2O_3 paste. The Al_2O_3 paste was ultrasonically dispersed for 2 h first and then stirred for 24 h. The Al_2O_3 films were fabricated on the TiO_2 compact layer using a doctor blade technique, and then were heated at 450 °C for 30 min. The annealed Al_2O_3 films were immersed into an aqueous solution of $TiCl_4$ (0.07 M) for post-treatment at 70 °C for 30 min.[20,21] Then, the Al_2O_3 films were flushed with deionized water, dried and annealed again at 450 °C for 30 min to form the A/T photoanode. The thickness of TiO_2 from A/T(n) photoanode could be adjusted by repeating cycles of the $TiCl_4$ treatment.

2.3. Fabrication of DSSCs

To eliminate the physisorbed water, the A/T photoanode was heated at 100 °C for 40 min and then immersed in ethanol solution of the N3 dye of 0.3 mM for 24 h. The dye-sensitized A/T photoanode together with a platinum foil counter electrode and liquid electrolyte composed of 0.5 M LiI, 0.02 M I_2, 0.3 M 1-methyl-3-hexylimidazolium iodide (HMII),[22] and 0.5 M 4-tert-butylpyridine in 3-methoxypropionitrile were assembled into a sandwich cell structure.

2.4. Characterization and measurements

The crystallographic structure of the A/T film was characterized by x-ray diffraction (XRD) (Rigaku D/max-2500) Cu Kα radiation with a scan speed of 8°/min. Surface morphology studies were carried out by scanning electron microscopy (SEM, Hitachi S-4800, 15 kV) and high-resolution transmission electron microscopy (HR-TEM, Tecnai G2 20 S-TWIN, 200 kV). The electrochemical performance was investigated by a Keithley 2611 Source Meter (Keithley Instruments, Inc., USA) under AM 1.5 (100 mW·cm^{-2}) supplied by a solar simulator (Oriel, 91160–1000). Electrochemical impedance spectroscopy (EIS) data were obtained under 100 mW·cm^{-2} illuminations, using a perturbation of ±10 mV over the open-circuit potential by using Solartron 1255B frequency analyzer and Solartron SI 1287 electrochemical interface system. The intensity-modulated photocurrent and photovoltage spectroscopy (IMPS and IMVS) were performed using a green light emitting diode (max = 520 nm) driven by a solartron 1255B frequency-response analyzer. The LED provided both the dc and ac components of the illumination. The UV spectrum measurement was made with aU-3010 spectrophotometer (Hitachi Corp).

3. Results and discussion

3.1. XRD analysis

Figure 1 shows the XRD patterns of FTO, Al_2O_3 film, and A/T(4) film. It can be seen that the diffraction peaks of 25.64°, 35.18°, 43.5°, 52.66°, 57.68°, 66.56° can match well with the standard rhombohedron phase of Al_2O_3 (JCPDF No. 46-1212). Compared to the Al_2O_3 film, the diffraction peaks of 25.34°, 53.49°, 68.3°, 69.1° from A/T(4) film can be assigned to standard anatase phase of TiO_2 (JCPDF No. 21-1272). It is evident that TiO_2 particles can form on the Al_2O_3 particles by $TiCl_4$ post-treatment. The slight decrease in peak strength of Al_2O_3 may be due to the Al_2O_3 layer coated by the TiO_2 layer from $TiCl_4$ hydrolysis, which weakens the relative strength.

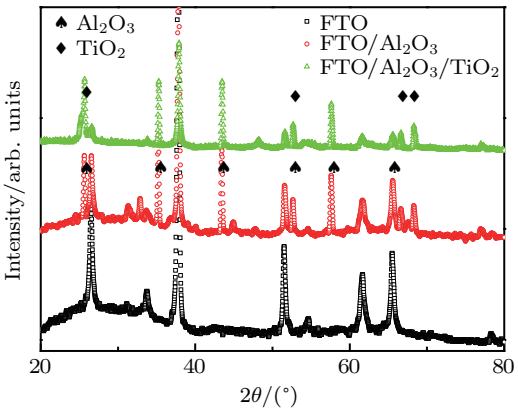


Fig. 1. (color online) XRD patterns of FTO, Al_2O_3 film, and A/T(4) film.

3.2. Morphology of A/T(n)

The Morphology of the Al_2O_3 film and the A/T(n) film is investigated by SEM and TEM (Figs. 2 and 3). It can be seen that the surface of the Al_2O_3 film is relatively rough compared to the A/T(4) film. TiO_2 particles formed by $TiCl_4$ hydrolysis grow on the Al_2O_3 particles, which make the surface of Al_2O_3 film smooth. The diameter of Al_2O_3 particles measured from

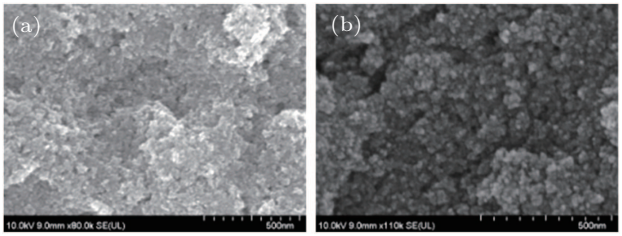


Fig. 2. SEM images of Al_2O_3 (a) and A/T(4) film (b).

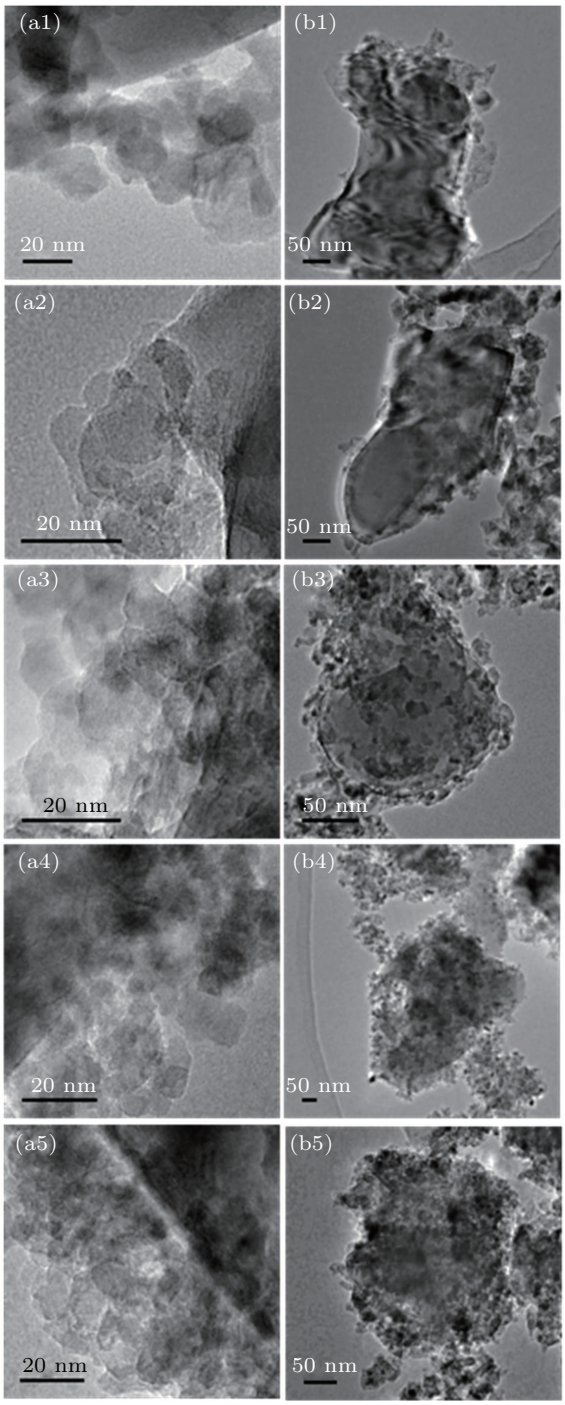


Fig. 3. TEM images of A/T(n) films.

the TEM image (shown in Fig. 3(a1)) is approximately 80 nm. As the time of $TiCl_4$ treatment increases, so does the number of TiO_2 particles and the diameter of TiO_2 is approximately 10–20 nm.

3.3. Photoelectric conversion properties

Dye adsorption increases from 2.11×10^{-7} mol·cm^{-2} of A/T(1) to 3.09×10^{-7} mol·cm^{-2} of A/T(4) only improve 50%. The Al_2O_3 films without $TiCl_4$ treatment also can adsorb dye on the Al_2O_3 particles with the value of 2.07×10^{-7} mol·cm^{-2}. Though Al_2O_3 can adsorb dye, Al_2O_3 cannot generate photocurrent because of its insulating properties. The increased surface area of the new TiO_2 particles formed on the Al_2O_3 surface is mostly canceled out by the overlap of TiO_2 on Al_2O_3 or overlap between TiO_2 particles. Dye adsorption falls to 2.49×10^{-7} mol·cm^{-2} for A/T(5) because the TiO_2 particles may block the channel and prevent the solution of dye connecting with the inner TiO_2 particles. The J_{sc} of A/T(1) is nearly zero, although the dye adsorption is quite large. The electrons neither inject into Al_2O_3 from adsorbed dye nor transfer in the network of Al_2O_3 to form photocurrent. The electrons can inject into TiO_2 from adsorbed dye but cannot transfer from one TiO_2 particles to another because of the isolation of TiO_2 particles. With the increase in $TiCl_4$ treatment times, the number of TiO_2 particles increases and, consequently, the particles are close to each other and form a conducting network. Electrons can transport in the network. Moreover, the increase in the number of TiO_2 particles formed on the surface of Al_2O_3 particles increases the amount of TiO_2 absorbing dye and reduces the amount of Al_2O_3 absorbing dye, which results in J_{sc} increasing remarkably to 7.79 mA·cm^{-2} with the increase in the $TiCl_4$ treatment times up to 4. However, J_{sc} is only 5.61 for A/T(5), owing to low dye adsorption and block of the contact between the dye and solution.

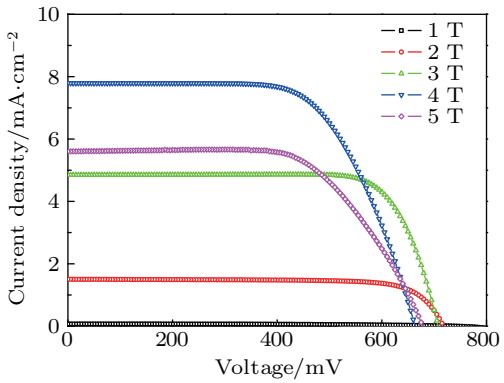


Fig. 4. (color online) I–V curve of A/T(n).

The V_{oc} of DSSC of A/T(n) has opposite trends compared to J_{sc} with the increase of n. The V_{oc} has the largest value of 745 mV for $n = 1$ and decreases with increasing n. The V_{oc} of A/T(4) is the smallest and only 655 mV. If we increase n to 5, the V_{oc} of A/T(n) increases again. Generally, the V_{oc} is determined by the difference of conduction and redox potential of the electrolyte, and the electron recombination rate. The dye

absorption may represent the surface area of TiO_2. From the dye absorption data, we know that A/T(4) has largest surface area. The larger the surface area is, the higher recombination rate is. Thus, the J_{sc} and V_{oc} of A/T(n) display opposite behavior with increase in n.

Table 1. Photoelectric conversion parameters of A/T(n).

Sample	J_{sc}/mA·cm^{-2}	V_{oc}/mV	ff	PCE/%	Dye loading /10^{-7} mol·cm^{-2}
A/T(1)	0.07	745	0.517	0.03	2.11
A/T(2)	1.51	715	0.767	0.82	2.16
A/T(3)	4.85	705	0.773	2.64	2.64
A/T(4)	7.79	655	0.651	3.32	3.09
A/T(5)	5.61	675	0.629	2.38	2.49

The FF of A/T(n) reduces with the increase in n. The low value of A/T(1) may be due to the large error caused by the low value of J_{sc}.

The J_{sc} of A/T(4) is higher than all of other treatment times, although V_{oc} and FF of A/T(4) are slightly lower than all of other treatment times. We obtained the highest PCE of 3.32% of A/T(4).

3.4. IMPS and IMVS

IMPS and IMVS of A/T(n) ($n = 1$–5) are shown in Fig. 5. Electron transport time (τ_t) in A/T(n) is calculated from the frequency of the lowest point in the IMPS plot and listed in Table 2. τ_t represents average time of electrons transport from injecting into TiO_2 to reaching the external circuit. The smaller the value of τ_t is, the faster the electron transfer rate is. The highest J_{sc} is in accordance with the shortest τ_t (2.02 ms) obtained from A/T(4). However, the amplitude of τ_t change is less obvious than the J_{sc} change from A/T(1) to A/T(5) (Tables 1 and 2). Hence, the rise of J_{sc} is only partly due to the increase of electron transfer rate. The formation of the conducting network of TiO_2 particles may also affect the J_{sc}. From the TEM images, it can be seen that TiO_2 particles become more and more and closely linked to constitute a conducting network with the increase times of $TiCl_4$ treatment. The expanding scope of conducting network causes the significant rise in the J_{sc} from A/T(1) to A/T(4). At the same time, the increasing TiO_2 particles in the conducting network can also enhance τ_t. Because TiO_2 particles connect to each other closely to form more routes for electron transport that make the electrons injected into the TiO_2 particles reach the substrate easier. Therefore, the electron transport in the network can choose a short path directly to the substrate and we get a very short τ_t in A/T(4). For A/T(5), TiO_2 particles may block the channel of electrolyte, and the ion in the electrolyte cannot transport alone with electrons to keep the electric neutrality. The movement of an electron would form an electrical field against the transport of electrons, resulting in the decrease in τ_t.

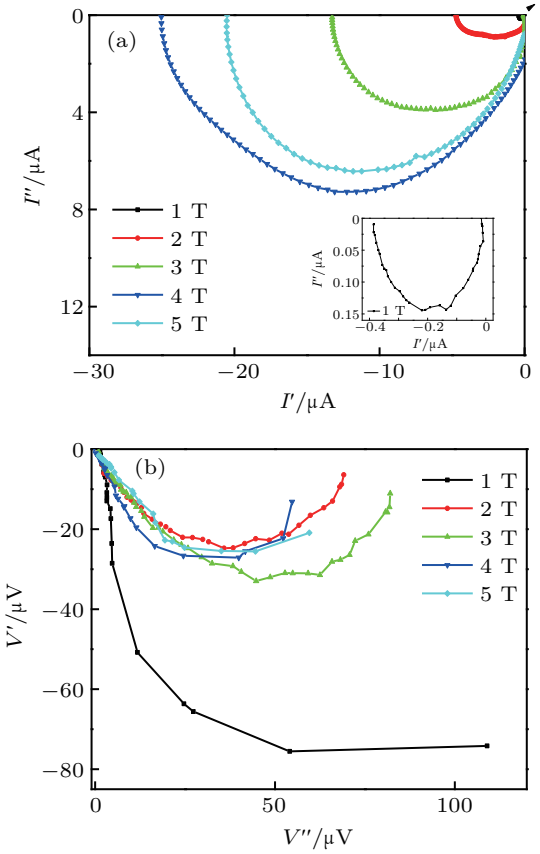


Fig. 5. (color online) (a) IMPS and (b) IMVS plot of A/T(n).

Table 2. Electron transportation time and lifetime.

Sample	$f_{min(IMPS)}$	$f_{min(IMVS)}$	τ_t/ms	τ_n/ms
A/T(1)	34.033	0.229	6.64	815.44
A/T(2)	35.397	0.891	4.5	178.67
A/T(3)	42.14	0.398	3.79	399.97
A/T(4)	79.771	0.336	2.02	555.31
A/T(5)	50.332	0.22	3.21	723.8

For A/T(1) or A/T(2), the conducting network is sparse, and electrons must be transported over a long curved path to reach the electrode, which increases τ_t. However, TiO_2 particles on the top of electrode are difficult to connect to the network, and most of TiO_2 particles in the network are close to the FTO electrode. Therefore, τ_t of A/T(1) or A/T(2) is less than 3 times of that of A/T(4).

Generally, electron transport in nanocrystalline is slower than in bulk materials. Compared with pure TiO_2 nanocrystalline film, TiO_2 particle in A/T(n) is smaller, and the transport length is longer owing to the Al_2O_3 core blocking the conducting path. However, the τ_t of A/T(n) is the same magnitude as pure TiO_2 films. The volume of TiO_2 particles is smaller than that of pure TiO_2 films, and the electron density in TiO_2 of A/T(n) is higher. High electron density may fill the trap state and accelerate the electron transfer rate.

The electron lifetime τ_n in A/T(n) is also calculated from the frequency of the lowest point in IMVS plot and listed in Table 2. τ_n represents the average time of electrons staying in

TiO_2 particles before they recombine with electrolyte or oxidized dye. Generally, longer τ_n means larger V_{oc}. However, this relation is not clear in our experiments. A/T(2) has shortest electron lifetime, but its V_{oc} is not the smallest, and only slightly smaller than A/T(1). We think that the IMVS measurement may has some error on A/T(2) and A/T(3).

3.5. EIS

The Nyquist plot of A/T(1–5) is shown in Fig. 6. In the Nyquist plot, EIS is composed of two semicircles. The interception of the high-frequency semicircle with the X-axis represents the serial resistance (R_s) of the cell, which consists of the resistance of electrolyte, FTO film, and TiO_2 working electrode. $TiCl_4$ treatment does not affect the resistance of electrolyte and FTO film. The variation of R_s with treatment times is due to the change in the resistance of working electrode, because the increased number of TiO_2 particles provides a better conducting network and reduces the serial resistance of the working electrode. The high-frequency semicircle represents the impedance of the counter electrode, which has nothing to do with the working electrode investigated in this study, and has not been analyzed. The low-frequency semicircle represents the impedance of recombination on the interface of TiO_2 and the electrode. The increased number of TiO_2 particles has larger surface area, but may also block the electrolyte channel. Those two effects lead the R_r to first decrease and then increase after four times treatment.

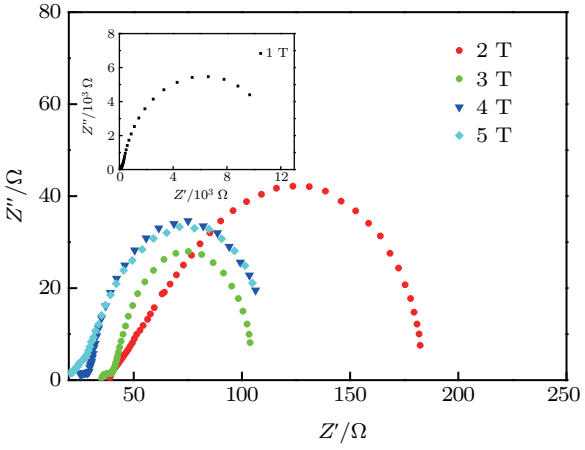


Fig. 6. (color online) EIS plot of A/T(n).

Table 3. Serial and recombination resistance of A/T(n).

Sample	R_s	R_r
A/T(1)	44.31	229.1
A/T(2)	38.83	51.98
A/T(3)	34.3	26.46
A/T(4)	24.81	29.37
A/T(5)	16.13	27.03

4. Conclusion and perspectives

TiO_2 nanoparticles were formed by $TiCl_4$ treatment on the framework of insulating Al_2O_3 nanoparticles of diameter 80 nm. The influence of various behaviors, such as photoelectrical, morphology, electron transport, and recombination, on the treatment times was investigated. With the increase in treatment times, the number of particles rather than diameter of particles were increased. J_{sc} and PCE reached peak at A/T(4) of 7.79 mA·cm^{-2} and 3.32% respectively. Electron transport time τ_t of A/T(n) obtained from IMPS measurement showed that $TiCl_4$ treatment times only slightly affected the τ_t, and its value was the same amplitude as pure TiO_2. Combining with TEM images of A/T(n), we thought that with the increase in n, the range and the inner connection of the conduction network was increased. The former increased the J_{sc}, and the later decreased the τ_t and serial resistance R_s. A/T(n) film provides a new model to understand the insight of electron transportation in semiconducting nanoparticles.

References

[1] Mahmoud S, Azam Iraji Z and Mehdi M 2014 *Chin. Phys. B* **23** 047302
[2] Wang H Y, Wang G S, Wu H J, Luo Y H, Li D M and Meng Q B 2016 *Acta Phys.-Chim. Sin.* **32** 201
[3] Xia R, Wang S M, Dong W W and Fang X D 2017 *Acta Phys.-Chim. Sin.* **33** 670
[4] Duan Y, Fu N, Liu Q, Fang Y, Zhou X, Zhang J and Lin Y 2012 *J. Phys. Chem. C* **116** 8888
[5] Wang M, Bai S, Chen A, Duan Y, Liu Q, Li D and Lin Y 2012 *Electrochim. Acta* **77** 54
[6] Fu N, Xiao X, Zhou X, Zhang J and Lin Y 2012 *J. Phys. Chem. C* **116** 2850
[7] Fang Y, Zhang J, Zhou X, Lin Y and Fang S 2012 *Electrochim. Acta* **68** 235
[8] Li X, Wang C, Xia N, Jiang M, Liu R, Huang J, Li Q, Luo Z, Liu L, Xua W and Fang D 2017 *J. Mol. Struct.* **1148** 347
[9] Zhang Q, *et al.* 2008 *Angew Chem. Int. Ed. Engl.* **47** 2402
[10] Ko S H, Lee D, Kang H W, Nam K H, Yeo J Y, Hong S J, Grigoropoulos C P and Sung H J 2011 *Nano Lett.* **11** 666
[11] Memarian N, Concina I, Braga A, Rozati S M, Vomiero A and Sberveglieri G 2011 *Angew Chem. Int. Ed. Engl.* **50** 12321
[12] McCune M, Zhang W and Deng Y 2012 *Nano Lett.* **12** 3656
[13] Xu C and Gao D 2012 *J. Phys. Chem. C* **116** 7236
[14] Zhang R, Pan J, Briggs E P, Thrash M and Kerr L L 2008 *Sol. Energ. Mat. Sol. C* **92** 425
[15] Birkel A, Lee Y G, Koll D, Van Meerbeek X, Frank S, Choi M J, Kang Y S, Char K and Tremel W 2012 *Energ. Environ. Sci.* **5** 5392
[16] Gubbala S, Russell H B, Shah H, Deb B, Jasinski J, Rypkemac H and Sunkara M K 2009 *Energ. Environ. Sci.* **2** 1302
[17] Tetreault N, ArsenaultÉ, Heiniger L, Soheilnia N, Brillet J, Moehl T, Zakeeruddin S, Ozin G A and Grätzel M 2011 *Nano Lett.* **11** 4579
[18] Snaith H J and Ducati C 2010 *Nano Lett.* **10** 1259
[19] Gao C, Li X, Lu B, Chen L, Wang Y, Teng F, Wang J, Zhang Z, Pan X and Xie E 2012 *Nanoscale* **4** 3475
[20] Sommeling P M, O'Regan B C, Haswell R R, Smit H J P, Bakker N J, Smits J J T, Kroon J M and van Roosmalen J A M 2006 *J. Phys. Chem. B* **110** 19191
[21] Zhong M, Shi J, Zhang W, Han H and Li C 2011 *Mater. Sci. Eng. B* **176** 1115
[22] Bonhote P, Dias A, Armand M, Papageorgiou N, Kalyanasundaram K and Grätzel M 1998 *Inorg. Chem.* **37** 166